Combined inhibition of RNA polymerase I and mTORC1/2 synergize to combat oral squamous cell carcinoma

Shanwei Shi[a], Huigen Luo[a], Lihong Wang[a], Hua Li[b], Yujie Liang[a], Juan Xia[a], Zhi Wang[a], Bin Cheng[a], Linfeng Huang[c], Guiqing Liao[a,*], Baoshan Xu[a,*]

[a] *Hospital of Stomatology, Guangdong Provincial Key Laboratory of Stomatology, Guanghua School of Stomatology, Institute of Stomatological Research, Sun Yat-sen University, Guangzhou, Guangdong Province, China*

[b] *The Stowers Institute for Medical Research, Kansas City, Missouri, United States* [c] *Division of Natural and Applied Sciences, Duke Kunshan University, Kunshan, Jiangsu, China*

ARTICLEINFO

Keywords:
Oral squamous cell carcinoma (OSCC) Ribosomal DNA (rDNA)
RNA polymerase I (RNAPI)
Mammalian target of rapamycin (mTOR) DNA damage and repair
Reactive oxygen species (ROS)

ABSTRACT

Oral squamous cell carcinoma (OSCC) is the major cause of morbidity and mortality in head and neck cancer patients worldwide. This malignant disease is challenging to treat because of the lack of effective curative strategies and the high incidence of recurrence. This study aimed to investigate the efficacy of a single and dual approach targeting ribosome biogenesis and protein translation to treat OSCC associated with the copy number variation (CNV) of ribosomal DNA (rDNA). Here, we found that primary OSCC tumors frequently exhibited a partial loss of 45S rDNA copy number and demonstrated a high susceptibility to CX5461 (a selective inhibitor of RNA polymerase I) and the coadministration of CX5461 and INK128 (a potent inhibitor of mTORC1/2). Combined treatment displayed the promising synergistic effects that induced cell apoptosis and reactive oxygen species (ROS) generation, and inhibited cell growth and proliferation. Moreover, INK128 compromised NHEJ- DNA repair pathway to reinforce the antitumor activity of CX5461. *In vivo*, the cotreatment synergistically suppressed tumor growth, triggered apoptosis and strikingly extended the survival time of tumor-bearing mice. Additionally, treatment with the individual compounds and coadministration appeared to reduce the incidence of enlarged inguinal lymph nodes. Our study supports that the combination of CX5461 and INK128 is a novel and efficacious therapeutic strategy that can combat this cancer and that 45S rDNA may serve as a useful indicator to predict the efficacy of this cotreatment.

1. Introduction

Oral squamous cell carcinoma (OSCC) is a major cause of morbidity and mortality in head and neck cancers worldwide, with an annual approximate incidence of 300,000 new cases [1]. OSCC is characterized by malignant metastasis and early recurrence [2]. A large number of OSCC tumors are diagnosed at a late clinical stage along with aggressive regional invasion. The commonly used therapeutic strategies for OSCC are surgery, chemotherapy and radiation therapy. Although therapeutic strategies have been actively studied in the past few decades, the 5-year survival rate of OSCC is still less than 50 %, and these patients often have a poor prognosis because of lymph node metastasis [3,4]. Therefore, developing a novel effective therapeutic strategy is an urgent medical necessity for OSCC patients.

The mammalian target of rapamycin (mTOR), a serine/threonine kinase, lies downstream of the type 1 insulin-like growth factor receptor (IGF-1R)-phosphatidylinositol 3′ kinase (PI3K) [5]. Typically, mTOR forms at least two complexes—mTORC1 and mTORC2—in mammalian cells [6]. mTORC1 regulates the phosphorylation of p70 S6 kinase 1 (S6K1) and eukaryotic initiation factor 4E (eIF4E) binding protein 1 (4EBP1) [7–13], whereas mTORC2 phosphorylates Akt (S473). Both mTORC1 and mTORC2 can be inhibited by ATP-competing kinase inhibitors, such as sapanisertib (INK128, which is in a phase I clinical trial for renal cell carcinoma and endometrial cancer, NCT01058707) [14,15]. Recent studies have revealed that the mTOR pathway is frequently upregulated in more than 80 % of head and neck squamous cell carcinoma (HNSCC) cases due to mutations of genes (*e.g.*, *PTEN, PIK3CA*) [16,17], resulting in aberrant activation of ribosome biogenesis and protein translation. Several small molecule inhibitors of mTOR signaling have been studied for treatments of OSCC tumors, including Temsirolimus [18], rapamycin [19], PF-04691502 [20], RAD001 [21, 22], metformin [23], and INK128 [24]. These reports prompted us to study how inhibition of mTOR signaling can effectively treat OSCC.

Ribosomal DNA (rDNA) encodes several functional ribosomal RNAs (rRNAs), which form ribosomes. Three of the four rRNAs are transcribed initially as a single transcript by RNA polymerase I (RNAPI) [25]. The repeats encoding the rRNAs are present at five different regions on human acrocentric chromosomes, with each region composed of several copies of the gene 45S rDNA. A single RNA transcript of 45S rDNA is processed into three separate rRNAs: 28S, 5.8S, and 18S [26]. The fourth rRNA is encoded by 5S rDNA, located on human chromosome I and

Abbreviations: HNSCC, head and neck squamous cell carcinoma; rDNA, ribosomal DNA; CNV, copy number variation; RNAPI, RNA polymerase I; RNAPII, RNA polymerase II; RNAPIII, RNA polymerase III; mTOR, mammalian target of rapamycin; rRNA, ribosomal RNA; RT-qPCR, quantitative reverse transcription PCR; RAPA, Rapamycin; EVER, Everolimus; HR, homologous recombination; NHEJ, nonhomologous end joining; TNM, tumor, nodes, metastasis; ROS, reactive oxygen species; DDR, DNA-damage response; DSB, double-strand breaks; DOK, human oral mucosa precancerous cells; NOK, normal oral keratinocyte cells.

* Corresponding authors.
E-mail addresses: drliaoguiqing@hotmail.com (G. Liao), xubsh3@mail.sysu.edu.cn (B. Xu).

https://doi.org/10.1016/j.biopha.2020.110906
Received 23 May 2020; Received in revised form 13 October 2020; Accepted 16 October 2020
Available online 13 November 2020
0753-3322/© 2020 The Authors. Published by Elsevier Masson SAS. This is an open access article under the CC BY-NC-ND license (http://creativecommons.org/licenses/by-nc-nd/4.0/).

transcribed by RNA polymerase III (RNAPIII) [27]. The malignant growth and metastasis of many tumors are closely associated with the upregulation of rDNA transcription and abnormal nucleolar morphology [28]. As a potent RNAPI inhibitor, CX5461 acts as a DNA intercalator [29]. CX5461 is a promising therapeutic approach for Myc-driven leukemia [30,31] and lymphoma [32]. In addition, CX5461 serves as a G-quadruplex stabilizer and blocks replication forks, which triggers single-stranded DNA breaks in BRCA1/2 mutated-cancers [33]. A recent study reported that CX5461 may induce its cytotoxic effect *via* topoisomerase II poisoning [34]. Clinically, CX5461 is in phase I/II trials for treating advanced hematologic malignancies (NCT02719977). Although Myc activity plays an important role in OSCC progression and invasion [35,36], the antitumor effect of CX5461 on OSCC tumors has remained elusive to date.

Our former study revealed that leukemia stem cells with PTEN deficiency and mTOR overexpression exhibit a decrease in 45S rDNA copy number [37]. Other studies have recently reported that ATRX-mutant human ALT (alternative lengthening of telomeres)-positive tumors exhibit a substantially lower rDNA copy number and are more sensitive to CX5461 treatment [38,39]. Therefore, the evidence indicates that the overactivation of mTOR signaling predisposes cells to a reduction in rDNA copy number that is associated with sensitivity to CX5461. However, rDNA CNV and its effect on OSCC treatment remain largely unknown. Here, we hypothesized that the combined inhibition of rDNA transcription and mTORC1/2 may effectively suppress OSCC tumors, and rDNA copy loss could improve susceptibility to this therapeutic approach.

In the study, we assessed a single and dual inhibition of ribosome biogenesis and protein translation using CX5461 and INK128 in OSCC cell lines, primary tumors, and a mouse cancer model. We found a robust synergistic effect of the combined treatment for OSCC *in vitro* and *in vivo*. INK128 remarkably inhibited the NHEJ-DNA repair pathway to enhance the antitumor activity of CX5461. Moreover, primary OSCC tumors and the adjacent normal tissues from the same individual patient were analyzed *via* whole-genome DNA sequencing. We found a frequent reduction of 45S rDNA copy number in primary tumors, which was associated with a high susceptibility to CX5461 treatment and the coadministration of CX5461 and INK128.

2. Materials and methods

2.1. Cell culture and reagents

Human oral normal and cancer cell lines, including normal oral keratinocyte (NOK), DOK, HOK, Cal33, SAS, SCC9, SCC15, SCC25, UM1, HSC3 and HSC6, were obtained from the American Type Culture Collection (ATCC) and Guangdong Provincial Key Laboratory of Stomatology, Guanghua School of Stomatology, and Hospital of Stomatology at Sun Yat-sen University. The cells were cultured in Keratinocyte SFM and DMEM-F12 medium (HyClone, Logan, UT, USA) with 10 % fetal bovine serum (FBS) (HyClone, Logan, UT, USA), 100 U of penicillin G/mL and 100 μg of streptomycin/mL (Sigma-Aldrich, USA) at 37 °C in a humidified atmosphere of 5% CO_2.

N-acetyl-L-cysteine (NAC) was purchased from Beyotime Institute of Biotechnology. Sapanisertib (INK128), rapamycin (RAPA), everolimus (RAD001) and CX5461 were purchased from Med Chem Express (San Diego, CA, USA). For the *in vitro* study, CX5461 was dissolved and stored as 10 mM stock solutions in PBS (vehicle). INK128, RAPA and RAD001 were dissolved and stored in 10 mM DMSO. For the *in vivo* study, CX5461 and INK128 were administered every 3 days at 30–40 mg/kg in PBS and 5 mg/kg in PBS.

2.2. Cell proliferation assay

Growth inhibition of the cancer cells was assessed using the CCK-8 assay. The cells were seeded into 96-well plates at 1 × 10^4 cells per well. After 24 h of culture, the media were replaced by vehicle or the compounds. The cells were incubated at 37 °C for 5 days. Then, 10 % CCK-8 (Dojindo Laboratories, Kumamoto, Japan) was added to each well. After 1 h of incubation, luminescence was measured at 450 nm using a microplate reader.

2.3. Cell apoptosis assay

Apoptosis assays were performed using flow cytometry analysis. The cells were cultured at a density of 5 × 10^5 cells in six-well plates. After 24 h, the cells were treated with the different compounds for 48 h. The cells were then collected at a density of 1 × 10^6 cells/mL in PBS. Then, annexin V-FITC and propidium iodide (PI) staining were performed according to the manufacturer's protocol (BD Biosciences, Franklin Lakes, NJ, USA). The tubes were gently mixed and incubated for 15 min at room temperature in the dark. The samples were analyzed using flow cytometry within 1 h. Unstained cells were used as a negative control.

2.4. Cell cycle analysis

The cells were cultured as described above. The cells were washed with PBS and centrifuged for 5 min at 1200 r.p.m., and ice-cold 70 % ethanol was added to fix the cells. The fixed cells were then incubated overnight at 4 °C. The next day, the cell pellet was incubated in 1 mL of PI (BD Biosciences, Franklin Lakes, NJ, USA) solution (50 μg/mL PI and 100 μg/mL RNaseA) at 25 °C room temperature (RT) for 30 min. The samples were analyzed using flow cytometry within 1 h. The results were analyzed using FlowJo V10 software to determine the distribution of different cell cycle phases. *2.5. Single-cell colony-formation assay*

For the single colony-formation assay, the cancer cells were plated into six-well plates at a density of 100 cells per well. After 24 h of culture, different compounds were incubated in the medium for 3 days. After 10 days, single-cell colonies were fixed and stained with 2 mg/mL methylene blue dissolved in methanol (0.5 %). The average efficiency of colony formation was normalized to assess the

sensitivity of the tumor cells for the indicated treatments.

2.6. Immunofluorescence staining

The tumor cells grown on confocal dishes were fixed in 4% paraformaldehyde for 20 min. The cells were then permeabilized in 0.5 % Triton X-100 for 10 min, blocked in 5% nonfat milk for 1 h, and washed with PBS three times. The cells were incubated with anti-phospho H2AX and anti-fibrillarin antibodies overnight at 4 °C, washed in PBS, and incubated with the secondary antibody at RT for 2 h. The cells were washed in PBS three times and counterstained with 4′6-diamidino-2- phenylindole (DAPI). The fluorescence images were captured with laser scanning confocal microscopy.

Table 1
Oligo primers for RT-qPCR.

Gene	Species	Direction	Sequence
β-Actin	Human	Forward	CGTCACCAACTGGGACGAC
		Reverse	A CTTCTCGCGGTTGGCCTTG G
18S pre-rRNA	Human	Forward	AAA CGG CTA CCA CAT
		Reverse	CCA CCT CCA ATG GAT CCT CGT

2.7. Quantification of cellular ROS levels

The cancer cells were treated with the indicated treatments and stained with 1 mM dihydroethidium (DHE) bromide for 30 min at 37 °C in the dark. The samples were then washed with PBS, and cellular ROS levels were measured by flow cytometry.

2.8. Protein immunoblotting

After each treatment, the cancer cells were lysed at 4 °C for 30 min in cooled RIPA buffer with 1% proteinase inhibitor and a phosphatase inhibitor cocktail. After the samples were centrifuged at 15,000 rpm for 30 min at 4 °C, the supernatants were collected. Protein content was detected using the Pierce BCA Protein Assay Kit (Bio-Rad, Richmond, CA, USA). Then, each sample was mixed 3:1 with 4× loading buffer and heated to 100 °C for 5 min. The lysates were separated by SDS-PAGE, transferred to polyvinylidene fluoride (PVDF) membranes (Bio-Rad, Hercules, CA), blocked with 5% milk for 1 h at RT and incubated with appropriate dilutions of the indicated primary antibodies overnight at 4 °C. The membranes were incubated with anti-mouse or anti-rabbit IgG antibodies conjugated to horseradish peroxidase at RT for 1 h; then, an ECL Plus Western Blotting Detection System (Amersham Biosciences, Piscataway, NJ, USA) was used for chemiluminescent visualization. The details of all antibodies are provided in Table S2.

2.9. Quantitative reverse transcription PCR

Quantitative reverse transcription PCR (RT-qPCR) was performed using the One-Step PrimeScript Probe RT-qPCR Kit (Takara Bio, Inc., Kusatsu, Japan). Total RNA was extracted by TriZol reagent and detected using a spectrophotometer. First-strand cDNA was prepared from total RNA using reverse transcriptase and oligo (dT) primers, and glyceraldehyde-3-phosphate dehydrogenase (GAPDH) was used as the internal control. qPCR was performed on an ABI 7900 H T System using the primers and probes listed in Table 1. Relative cDNA expression levels were estimated with the ΔCt method and normalized to the GAPDH gene expression.

2.10. H3-uridine metabolic labeling to measure rRNA production

The tumor cells were labeled with H3-uridine (5 μCi) for the indicated amount of time (180 min) per sample. Total RNA was isolated with TRIzol Reagent (Invitrogen, USA) and the concentration of each RNA sample was measured by a Qubit RNA assay. One microgram of each sample was counted in a Beckman LS 6500 multipurpose scintillation counter to determine new rRNA production based on H3-uridine incorporation.

2.11. Animal experimentation ethics

All animal experiments were performed according to protocols approved by the Sun Yat-sen University Animal Ethics Committee, Sun Yat-sen University (Guangzhou, China).

2.12. In vivo animal study

A total of 80 four-week-old BALB/c nude mice were purchased from Beijing experimental animal center and kept in specific pathogen-free (SPF) conditions. The animals were subcutaneously injected with 1 × 10^6 Cal33 cells (suspended in 100 μL of PBS), and after one week, the tumor-bearing mice were randomly divided into two sets of four groups. The control group was injected with PBS, and the three experimental groups were injected with CX5461 or INK128 alone or in combination every 3 days. Tumor growth was monitored using a caliper, and tumor volume was calculated according to the formula $V=\pi_{\times}$maximal diameter × perpendicular diameter 2/6. One set of four groups of animals was sacrificed after 27 days of administration, and specimens were collected. The tumor volume and tumor growth curves were established. The other set of four groups of animals was maintained after the 27-day treatment regimen, and survival time of the different groups of animals was recorded. *2.13. Tissue immunostaining*

The tumor tissues were fixed and sliced at a thickness of 4 μm using a pathological slicer (LEICA RM2145, Germany). The slices were dried, and hematoxylin and eosin (HE) staining, immunohistochemical staining, and terminal deoxynucleotidyl transferase-mediated dUTP nick end-labeling (TUNEL) fluorescence staining were performed using a fluorescence inversion microscope system (Zeiss, Germany).

2.14. Collection of clinical primary tissues

The primary tissue samples of the OSCC patients were unbiasedly obtained during surgery in the

hospital of stomatology at the Sun Yat- sen University using an approved institutional review board protocol (Sun Yat-sen University). The samples from patients who received preoperative radiation or chemotherapy were excluded. The clinical information of the OSCC patients is listed in Table S1. Primary tumors and the matching normal tissues were preserved in liquid nitrogen for subsequent detection. All patients were stochastically selected without any preference.

2.15. Whole-genome DNA sequencing

DNA-seq libraries were generated from 1 ng of genomic DNA as assessed by Qubit 2.0 Fluorometer (Life Technologies). Libraries were generated according to the manufacturer's directions for the Nextera XT Library Prep Kit (Illumina, Inc.) and purified using the Agencourt AMPure XP System (Beckman Coulter). The resulting libraries were checked for quality and quantity using LabChip GX (Perkin Elmer) and Qubit. Equal molar libraries were pooled, re-quantified and sequenced as 125 bp paired reads on the Illumina HiSeq 2500 instrument using HiSeq Control Software 2.2.58. Following sequencing, Illumina Primary Analysis version RTA 1.18.64 and Secondary Analysis version bcl2fastq2 v2.17 were run to demultiplex reads for all libraries and generate FASTQ files.

2.16. Computational analysis of cancer genome sequencing

The cancer genome datasets were obtained with whole-genome- sequencing of human primary OSCC tumors. The analysis method used for the rDNA copy number is similar to a previously published method [40]. Briefly, the human consensus 45S rDNA sequences were obtained from NCBI (accession: U13369). Reads were mapped to the 45S locus, and a set of 16,022 preselected putative single-copy exons (the largest from each gene) were identified using Bowtie2 v2.1.0 with the default parameters. Only concordant read pairs were kept in the downstream analysis. The rDNA copy numbers of 18S, 5.8S, and 28S were calculated as the mean coverage in the respective regions. To make samples comparable to each other, the rDNA copy number was further normalized to the background genome coverage, which was calculated as the median coverage of the single-copy exons.

For sequence analysis, the predominant sequence of each individual genome was compared to that of the human reference sequence for 45S. Each nucleotide position was either a match to the consensus 45S sequence, or if not a match, then the position was called a single nucleotide variation (SNV). SNVs in 45S rDNA region were called using SAMtools mpileup (v1.9) after the duplicated reads were removed from the aligned read files. SNVs were further filtered with the quality score (>20, "PASS"). If the SNVs of the cancer and normal matched genome pair were identical, this was termed a shared SNV. If the SNV was not identical, this position was termed a unique SNV. The mutation rate was calculated as the number of unique SNVs divide the feature length (28S or 45S rDNA). For the shared SNVs in a pair, each position was evaluated for sequence evidence of 1–4 different nucleotides. The allele numbers for the shared SNVs were used to calculate an average allele number for each genome. The average number of alleles at the shared SNVs for normal tissue was subtracted from that for tumor tissue to generate the allele

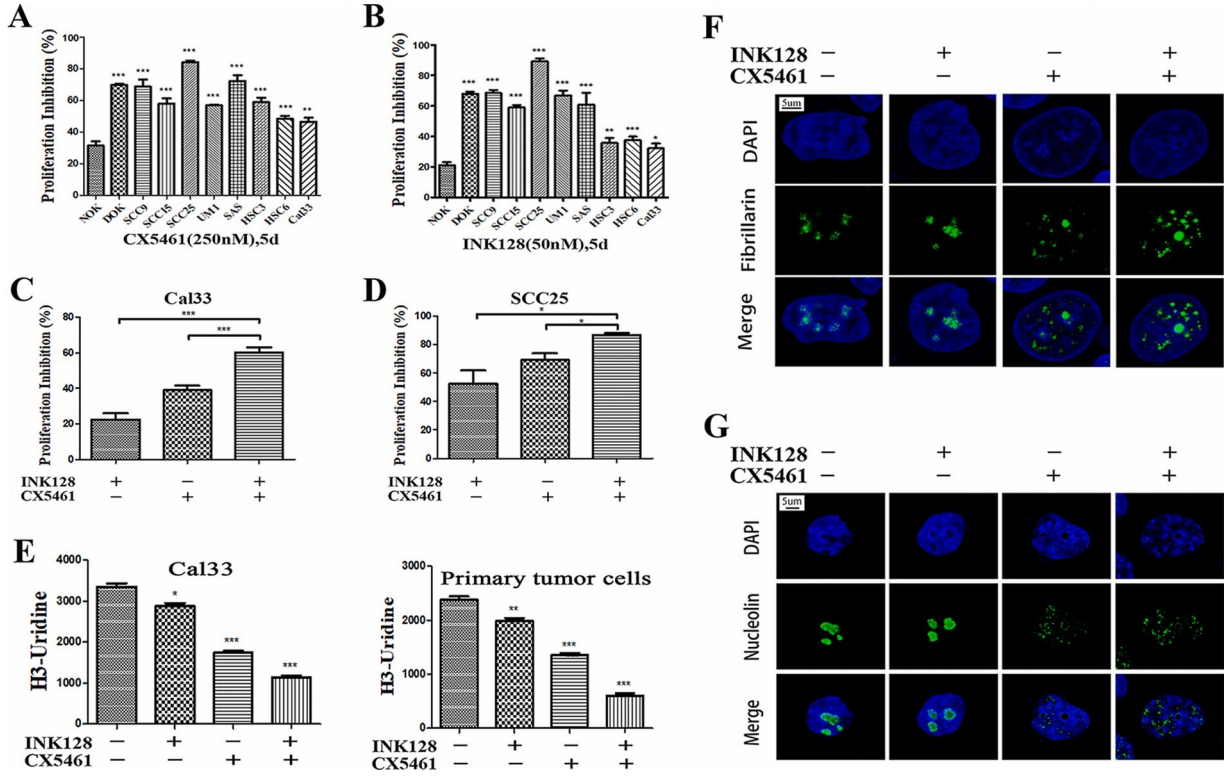

Fig. 1. The coadministration of CX5461 and INK128 was synergistic in the treatment of OSCC cells. (A-B) NOK, DOK, and a panel of OSCC cells were treated with 250 nM CX5461 (A) or 50 nM INK128 (B). Cell proliferation was measured by CCK-8 assay, and the percentages of proliferation inhibition were normalized to the DMSO control groups. (C-D) The proliferation inhibition of Cal33 (C) and SCC25 (D) cells was measured after the indicated treatments. The percentages of proliferation inhibition were normalized to the control groups treated with DMSO. **(E)** Global new rRNA production was measured after the indicated treatments by H3- uridine metabolic labeling in Cal33 cells and primary tumor cells. The unit for the Y-axis is CPM/μg RNA. (F-G) Nucleolar distributions of fibrillarin (F) and nucleolin (G) were assessed by immunofluorescence staining in OSCC tumor cells after the indicated treatments for 24 h. Scale bar: 5 μm.

difference for each matched pair, and the differences were plotted as individual points in the box plot.

2.17. Statistical analysis

The IBM SPSS 20.0 statistical software was used for statistical analysis. A two-tailed Student's *t*-test was used to analyze the difference between the drug treatment group and the control group. *In vitro* experiments were performed in triplicate and expressed as a summary of the mean of replicates with SD, unless specified otherwise. Histological quantitation of mouse tumor tissue was performed using an Aperio ScanScope digital scanner and viewed using ImageScope software (Leica Biosystems). All values are presented as the mean ± standard deviation (SD). p <0.05 was considered significant. All quantitative data represent the mean of at least three independent biological replicates.

3. Results

3.1. Combined inhibition of mTORC1/2 and RNAPI exhibited a cooperative effect on OSCC cells

First, Cal33 and HSC3 OSCC cells were treated with different concentrations of INK128 (mTORC1/2 inhibitor) and CX5461 (RNAPI inhibitor) for 5 days, followed by cell viability assay using a CCK-8 assay. As shown in Fig. S1A and B, INK128 and CX5461 inhibited cell viability of Cal33 and HSC3 cell lines in a dose-dependent manner. The half maximal inhibitory concentrations (IC50 s) of these two compounds were calculated from the inhibition curve. IC50 s of CX5461 were 547.8 nM at NOK cells, 201 nM at Cal33 cells, and 259.2 nM at HSC3 cells. IC50 s of INK128 were 381.6 nM at NOK cells, 65.3 nM at Cal33 cells, and 29.3 nM at HSC3 cells. The IC50 concentrations of these two compounds at NOK cells were much lower than OSCC cells, indicating that OSCC cells are more sensitive to the treatments than NOK cells. Therefore, we chose 250 nM CX5461 and 50 nM INK128 for the subsequent experiments. The OSCC cells were treated with CX5461 and INK128 for Western blotting analysis. We observed that INK128 markedly inhibited the phosphorylation of Akt (Ser473), RPS6 (Ser235/236), and 4EBP1 (Thr70) in Cal33 and HSC3 cells with a 3 -h treatment (Fig. S1C and D). The data indicated that both mTORC1 and mTORC2 signaling were obviously inhibited by INK128, but CX5461 did not affect Akt/mTOR signaling. On the next, a panel of human oral cell lines were exposed to INK128 (50 nM) and CX5461 (250 nM) for 5 days. In general, the inhibitory effects of INK128 and CX5461 were significantly stronger on the proliferation of various OSCC cell lines and DOK (precancerous oral tissue) than NOK (normal oral keratinocyte cells) as well (Fig. 1A and B). We have assessed the endogenous

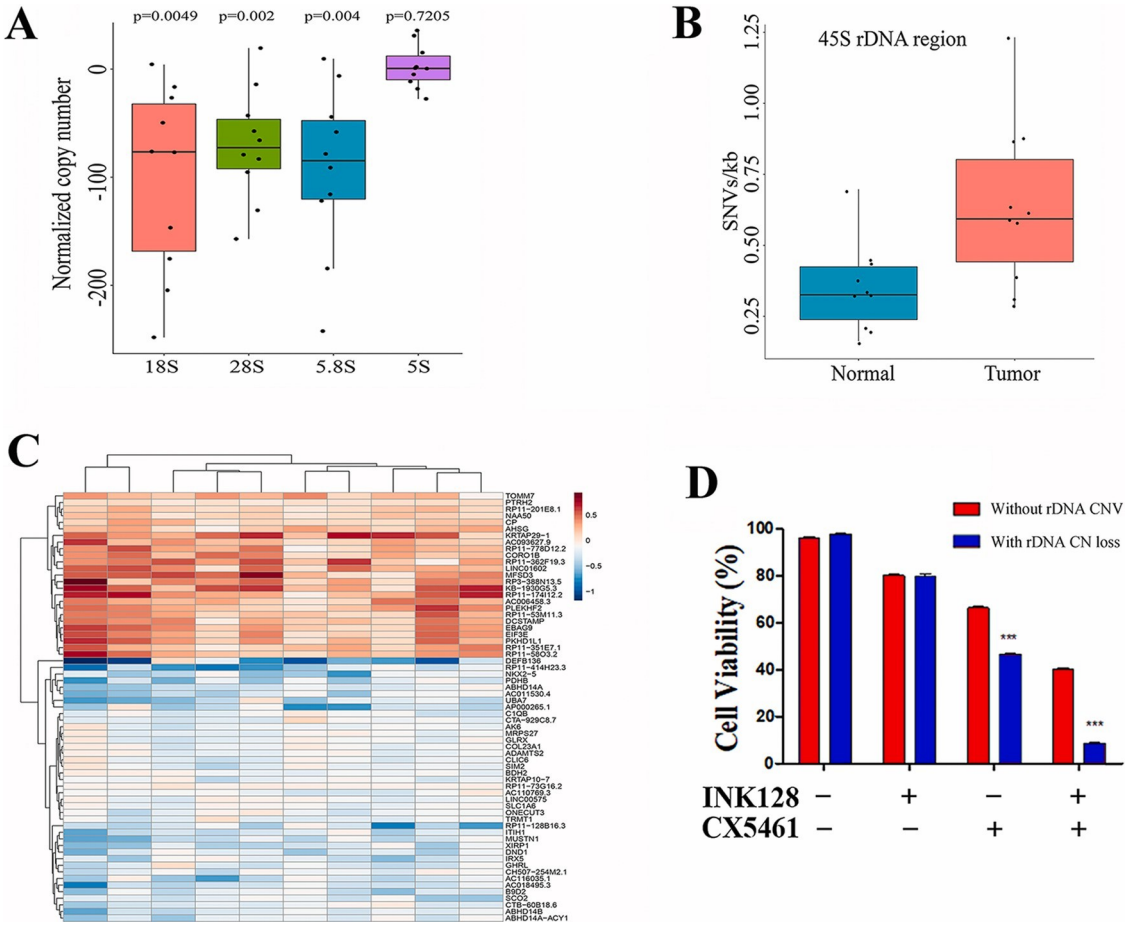

Fig. 2. The 45S rDNA copy number was frequently reduced in primary OSCC tumors. **(A)** Whole-genome DNA sequencing analysis of rDNA copy number in primary OSCC tumors. Normalized copy numbers of the 18S, 28S, 5.8S, and 5S rDNA regions are shown for the cancer genomes. Copy number (CN) of rDNA repeats was calculated by subtracting the CN of adjacent normal tissues from the CN of primary tumors (*, $p < 0.05$; **, $p < 0.01$; ***, $p < 0.001$; NS, not significant). **(B)** 45S rDNA regions in primary tumors exhibited more SNVs than their adjacent normal tissues. The p value is 0.01668 for the difference between primary tumors and matched normal tissues. **(C)** Copy number covariations in coding genes in primary OSCC tumors were associated with reduced rDNA copy number. The copy number of genes was calculated as the average coverage of a defined gene region using the normalized coverage in reads per million. The heatmap displayed the fold changes in copy number between primary tumors and matched normal tissues. **(D)** Using cell viability analysis, single and dual treatments of INK128 and CX5461 were assessed in primary OSCC tumors with or without the partial loss of 45S rDNA CN.

expression levels of Akt/mTOR signaling, and global new rRNA biogenesis in all of the cells as shown in Fig.S1E and F. The data have shown that endogenous levels of phosphor- Akt, phosphor-RPS6 and phosphor-4EBP1, and global rRNA production in OSCC cell lines and DOK (precancerous oral tissue) were generally stronger than NOK cells. In SCC25, HSC3 and Cal33 cell lines, the endogenous expression levels of phosphor-Akt, phosphor-RPS6 and phosphor-4EBP1 appeared to be higher. Moreover, global new rRNA production was significantly higher in SCC25, HSC3, Cal33, and SAS cells. Therefore, we primarily selected these cell lines to assess the antitumor mechanisms of RNAPI and mTOR inhibitors. We observed that the treatment cotargeting RNAPI and mTORC1/2 exerted the strongest suppressive effect on the proliferation of Cal33 (proliferation inhibition rate: 61.3 ± 3.7 %) and SCC25 cells (88 ± 1.6 %) compared to treatment with INK128 (Cal33, 22.5 ± 4.8 %; SCC25, 53.3 ± 8.8 %) or CX5461 alone (Cal33, 40.7 ± 2.9 %; SCC25, 69.5 ± 2.3 %) for 72 h (Fig. 1C and D). Typically, rRNAs are the most abundant composition of total RNAs. Because rRNA constitutes approximately 60 % of the total RNA made by actively growing cells, H3-uridine incorporation assay is commonly used to measure global new rRNA synthesis [41]. In Cal33 cells and primary OSCC tumor cells, CX5461 showed a more potent inhibition of new rRNA synthesis than did INK128, and the combined treatment showed stronger inhibitory effect on rRNA production than INK128 or CX5461 treatment alone (Fig. 1E). We also conducted qPCR analysis to determine the expression of 18S pre-rRNA, which displayed a similar tendency as the H3-uridine labeling study (Fig. S1G). We noticed that the efficiency of the inhibition by single-agent treatment (INK128 or CX5461) was similar to the 18S pre-rRNA levels. Based on some previous studies, mTOR signaling pathway can indirectly regulate the transcription and processing of 18S pre-RNA. Inhibition of mTOR signaling by rapamycin treatment not only leads to a rapid impairment of 18S rRNA gene transcription and 18S pre-rRNA processing but also induces its decay in human cells [42,43]. Thus, INK128 treatment displays a similar inhibitory effect for the 18S pre-RNA with CX5461. However, for global new rRNA synthesis, CX5461 exhibits a more specific inhibition than INK128 on RNAPI transcription. In Fig. 1E, CX5461 showed a stronger suppression of global new rRNA production than INK128. Moreover, a single-cell colony formation assay showed that colony growth of Cal33 and SAS cells were completely blocked by treatment of CX5461 and the cotreatment. However, INK128 only partially inhibited the colony
formation of these OSCC cells (Cal33, 66.2 ± 7.5 %; SAS, 57.9 ± 5.5 %) compared with the DMSO-treated

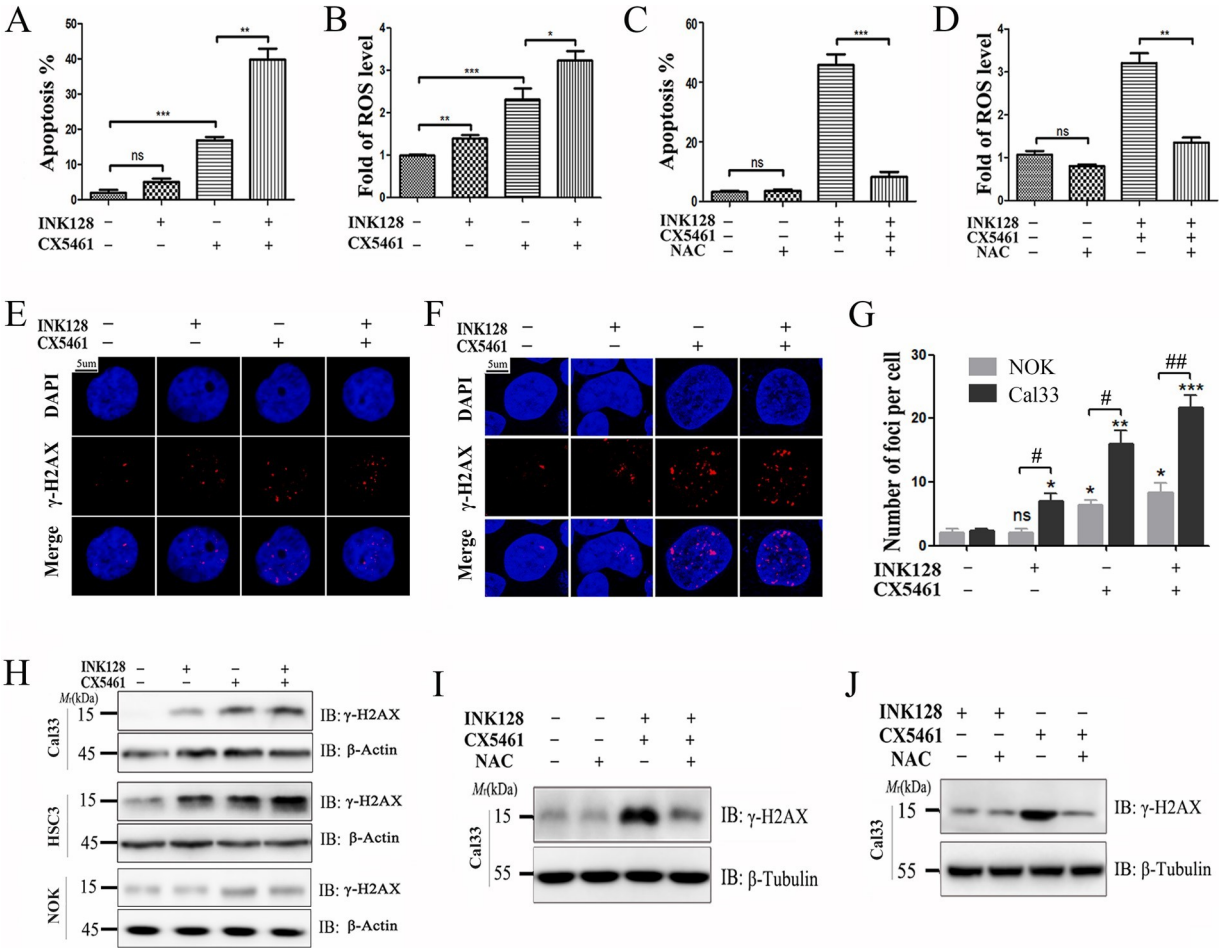

Fig. 3. INK128 and CX5461 synergistically induced apoptosis, oxidative stress, and DNA damage. **(A)** Annexin V and PI double-staining was used to measure apoptosis levels in Cal33 cells after the indicated treatments for 48 h. **(B)** Cellular ROS generation in tumor cells after the indicated treatments was measured by flow cytometry using an oxidation-sensitive fluorescent probe (DHE). **(C-D)** Apoptosis (C) and ROS generation (D) were measured in Cal33 cells after the combined treatment with or without NAC preincubation for 24 h. **(E-F)** The formation of γ-H2AX foci was monitored upon the indicated treatments in NOK (E) and Cal33 cells (F) for 24 h. Scale bar: 5 μm. **(G)** Quantitation of γ-H2AX foci formation after the indicated treatments in NOK (E, gray column) and Cal33 cells (F, black column). **(H)** Western blot analysis was performed using antibodies against γ-H2AX and β-Actin in Cal33, HSC3, and NOK cells after the indicated treatments for 24 h. **(I)** γ-H2AX expression levels were assessed by Western blot analysis in Cal33 cells treated with INK128 and CX5461 coadministration with or without NAC preincubation for 24 h. **(J)** γ-H2AX expression levels were assessed by Western blot analysis in Cal33 cells treated with INK128 or CX5461 with or without NAC preincubation for 24 h.

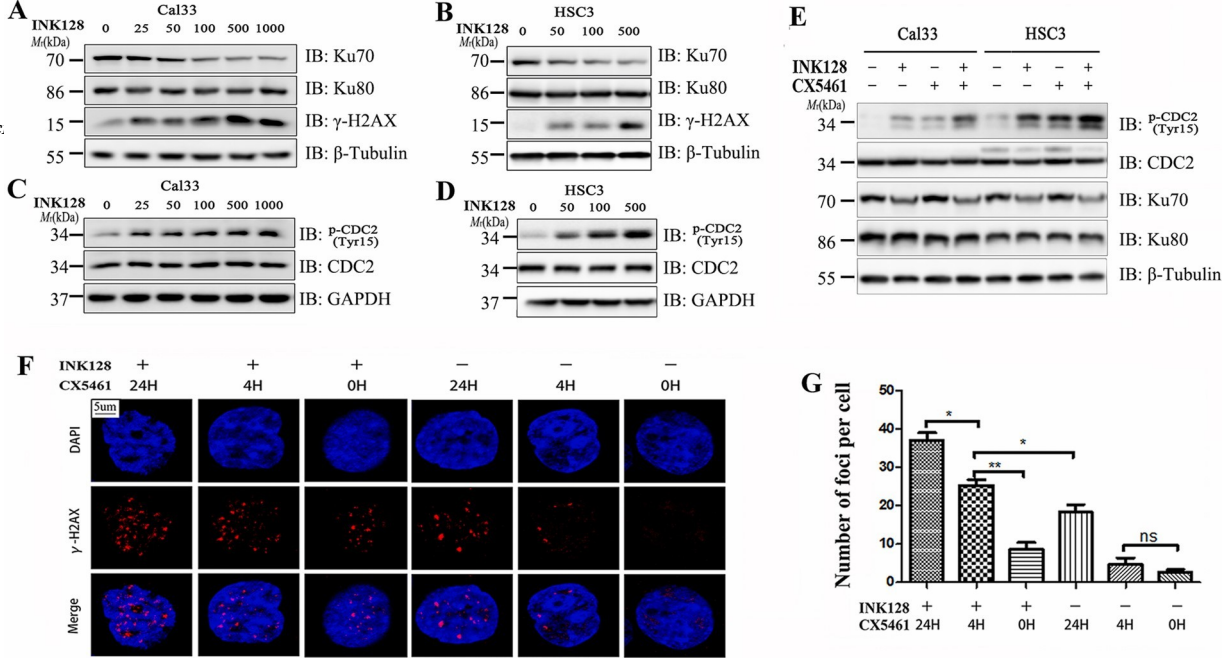

groups (Cal33, 95.6 ± 3.1 %; SAS, 97.3 ± 2.5 %) as shown in Fig. S1H and I. These data suggested that oral cancer cells may develop resistance to mTORC1/2 inhibitors due to tumor heterogeneity. Taken together, the cotargeting of mTORC1/2 and rDNA transcription synergized to suppress the growth and proliferation of OSCC cells.

Fibrillarin and nucleolin are two important nucleolus components for the synthesis, processing, modification and ribosome assembly of rRNA [8]. The data showed that CX5461 treatment resulted in the dispersal of nucleolus fibrillarin and nucleolin, while INK128 did not have any obvious effect on nucleolar organization (Fig. 1F and G). Intriguingly, INK128 significantly enhanced CX5461-induced disruption of nucleolus integrity through the quantitative analysis of fibrillarin and nucleolin loci per cell to validate their synergistic action on nucleolar damage (Fig. S2A and B). As reported, ribosomal DNA (rDNA) is crucial for nucleolus biogenesis, organization, and function. Nucleolar and rDNA may serve as organizers of chromatin territories to collaboratively affect heterochromatin maintenance, cell metabolism, aging, gene expression, and epigenetic states of the genome [38]. Because OSCC cells are highly susceptible to nucleolus damage and inhibition of rDNA transcription, we questioned how rDNA is variable and its effect on OSCC tumors. To address this question, we collected 10 pairs of primary OSCC tumors and the adjacent normal tissues for whole-genome DNA sequencing. We were able to avoid aneuploidy interference and count gene copy number accurately by whole-genome analysis based on the previous study [37]. The results showed that copies of 45S rDNA (including 18S, 28S and 5.8S) were frequently reduced by approximately 70 copies compared with the matched adjacent normal tissues (Fig. 2A). However, 5S rDNA copies were unchanged in the primary tumors, indicating that 5S rDNA CNV was independent of 45S rDNA.

Fig. 4. INK128 suppressed NHEJ-DNA repair pathway and cell cycle progression. **(A-B)** The protein expression levels of γ-H2AX and the NHEJ factors Ku70 and Ku80 were detected using Western blot analysis in Cal33 (A) and HSC3 (B) cells treated with INK128 for 24 h. β-tubulin was used as a loading control. **(C-D)** The protein expression levels of CDC2 and phosphor-CDC2 were determined using Western blot analysis in Cal33 (C) and HSC3 (D) cells treated with INK128 for 24 h. GAPDH was used as a loading control. Phosphorylated CDC2 levels in Cal33 and HSC3 cells were increased by INK128 treatment in a dose-dependent manner. **(E)** The protein levels of the NHEJ factors Ku70 and Ku80 and the cell cycle-regulatory protein CDC2 were detected by Western blot analysis after the indicated treatments for 24 h. **(F)** The DNA damage response (DDR) in OSCC tumor cells was detected by immunofluorescence analysis. SAS cells were treated with or without INK128, while tumor cells were treated simultaneously with either CX5461 or vehicle for 24 or 4 h. CX5461-24H indicates long-term treatment (24 h) with CX5461. CX5461-4H indicates short-term treatment (4 h) with CX5461, followed by replacement with fresh medium. **(G)** Quantification of γ-H2AX foci formation was analyzed after the indicated treatments in (F).

The human rDNA repeats are ~30 % transcribed (ETS, ITS, 18S, 5.8S, 28S) and ~70 % non-transcribed (IGS). Previous work has indicated that all non-coding regions of the human repeat can tolerate SNVs, including the 5′ and 3′ external transcribed spacer regions, the internal transcribed spacers, and the large intergenic region [37]. The 45S rDNA loci contain coding regions (18S, 5.8S, 28S) and non-coding regions (IGS, ITS1, ITS2, intergenic region). Here, we found that 45S rDNA loci have increased SNVs. Because the large non-coding regions have been reported to be highly variable, we further analyzed SNVs on 28S rDNA to determine sequence variation in the coding region. As expected, increased SNVs also occurred in 28S rDNA sequences (Fig. 2B and S2C). In the whole genome sequencing data, it is difficult to analyze SNVs in 5S rDNA region because of its strong background noise. These data indicated that the decrease in 45S rDNA copy number correlated with an increased variation of rDNA sequences. To further analyze gene copy number variation in the OSCC genome, we used the copy number of the preselected exons used for normalization to discover additional genes whose copy number co-varied with the ribosomal DNA. Exons were selected that displayed a significant copy number difference based on results of a paired *t*-test for all the tumors *versus* all the normal values for each exon for each genome (FDR< = 0.05). We then used hierarchical clustering to identify exons with similar trends in copy number (gain or loss) in the OSCC genome with low rDNA copy number in tumor *versus* normal. The “gain” cluster was with ~25 exons (red color, such as TOMM7, AHSG, KRTAP29 and EIF3E et al.), and the “loss” cluster was with ~40 exons (blue color, such as DEFB136, PDHB, and ITIH1 et al.). These exons are spread across all chromosomes and are not

confined to the chromosomes with 45S rDNA genes, indicating global rather than local structural variations accompany the loss of rDNA copies. The data suggested the increase and decrease in copy number of these genes could affect cellular physiology (Fig. 2C and Table S3). Subsequently, we selected the primary tissues for Western blot analysis and found that mTOR activity was indeed over-activated in primary OSCC tumors compared with the matching normal tissues (Fig. S2D). The results suggested that overexpression of mTOR signaling was associated with a partial loss of 45S rDNA copy number. A few studies have reported that approximately only half of 45S repeats are actively transcribed, although copy number of rDNA is highly variable between individuals [5,44,45]. Compared to primary OSCC cells without rDNA CNV (red color column, the cells were used from NO.8 OSCC patient in Table S1 with red font), the OSCC cells with reduced 45S rDNA CN (blue color column, the cells were used from NO.6 OSCC patient in Table S1 with blue font), exhibited a higher susceptibility to CX5461 (average cell viability: 48.2 %, p□0.001) than INK128 (average cell viability: 81.3 %, p = 1.00). The partial loss of 45S rDNA resulted in increased sensitivity to CX5461 and CX5461 + INK128 treatment in the primary OSCC cells (Fig. 2D). Interestingly, a combination of CX5461 and INK128 synergized to kill the primary tumor cells dramatically, especially in the OSCC cells with rDNA copy loss (average cell viability: 9.7 %, *p*□0.001).

3.2. INK128 and CX5461 synergistically induced oxidative stress, DNA damaging, and apoptosis

To further investigate the anticancer effects of the cotargeting treatment, we used flow cytometry analysis to detect apoptosis of OSCC cells with single-compound treatment and the cotreatment for 48 h (Figs. 3A and S3A). The results showed that CX5461 significantly induced cell apoptosis (apoptosis rate: 18.48 ± 5.52 % *vs.* 3.5 ± 0.6 % in the DMSO-treated group; *p*□0.001) rather than INK128 (apoptosis rate: 6.73 ± 1.45 %, *p* = 0.27). Remarkably, the coadministration induced higher levels of cell apoptosis (apoptosis rate: 39.84±8.72 %, *p* = 0.0042) than single-compound treatment. Some anticancer compounds are reported to induce accumulation of reactive oxygen species (ROS), which is a primary factor to trigger DNA-damage response (DDR) [9]. To date, no clear evidence has indicated that INK128 and CX5461 promote ROS generation to induce DNA damage and apoptosis. Here, our data showed that cellular ROS levels were induced significantly by both INK128 and CX5461, and CX5461 displayed a stronger induction than INK128. Notably, the combined treatment synergized to promote ROS generation (Figs. 3B and S3B). Subsequently, antioxidant N-acetylcysteine (NAC, 1 mM) was used to assess whether ROS generation was involved in the compound-induced apoptosis via 1 -h preincubation. As expected, the preincubation of NAC dramatically eliminated the combined treatment-induced apoptosis and ROS production (Figs. 3C-D, S3C and D). Although INK128 treatment moderately elevated cellular ROS levels, it did not significantly induce apoptosis, which indicated that INK128 mainly inhibited proliferation rather than the survival of OSCC

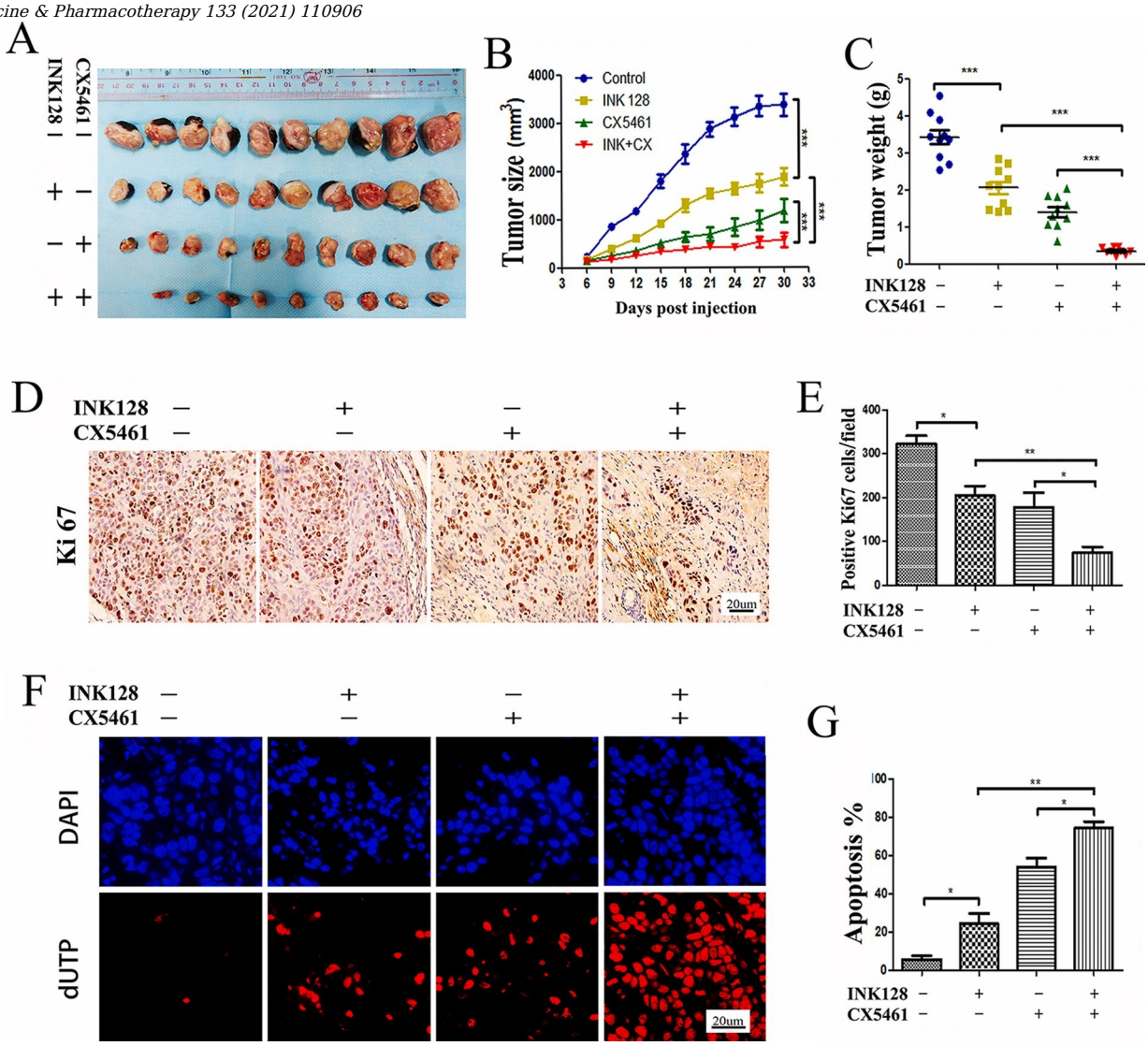

Fig. 5. Coadministration of CX5461 and INK128 was robustly synergistic against OSCC tumors *in vivo*. **(A)** The tumor sizes of the OSCC tumors were determined in these groups with the indicated treatments. **(B)** Growth curves of the xenograft tumors were generated for the groups with the indicated treatments. **(C)** The average weights of the xenograft tumors were measured in these groups with the indicated treatments on day 27. (D-E) Tumors subjected to immunohistochemistry (IHC) for Ki67 (D) were imaged, and the positive cells were quantitatively analyzed (E) in tumors with the indicated treatments. Scale bar: 20 μm. **(F)** The apoptotic cells were stained by dUTP immunofluorescence (IF) solution in tumors with the indicated treatments. DAPI was used for nuclear staining. Scale bar: 20 μm. **(G)** The percentages of dUTP IF-positive staining in (F) were quantitatively analyzed. The data were quantitatively analyzed using ImageJ software.

tumor cells. Another possibility is that INK128-induced ROS production may not reach the oxidative stress threshold to trigger apoptosis pathways, according to a previous report [10].

Genomic DNA damage is commonly attributed to cellular ROS, ionizing radiation, and certain chemotherapeutic agents [11]. To evaluate whether INK128 and CX5461 induce DNA-damage stress through ROS generation, we treated NOK and Cal33 cells with the two compounds. As shown in the Fig. 3E–H, individual and combined treatments of INK128 and CX5461 only mildly triggered γ-H2AX signaling in NOK normal oral cells, compared to their effects in OSCC cells. In NOK cells, the treatments-induced DNA damaging was much weaker than that in OSCCs. According to the data, the pro-apoptosis effect of CX5461 and INK128 is more cytotoxic towards the OSCC tumor cells rather than normal oral cells. The γ-H2AX signals were robustly induced by CX5461 in the OSCC cells, which is consistent with a recent study on CX5461 as a G-quadruplex stabilizer [33]. In addition, a slight γ-H2AX increase was also observed upon INK128 treatment (Fig. 3F–G). Especially, the combined treatment induced the strongest elevation of γ-H2AX signals. As predicted, the combined treatment-induced increase in γ-H2AX was significantly attenuated by NAC (1 mM) preincubation (Fig. 3I), indicating that oxidative stress mediated the DNA damage and apoptosis induced by the combined treatment. To further examine the roles of INK128 or CX5461 on DNA damage, INK128 and CX5461 were separately added with or without NAC preincubation (Figs. 3J and S3). NAC markedly prevented CX5461-induced γ-H2AX expression but had no impact on the effect of INK128. This result indicated that the induction of ROS generation by CX5461 mostly caused genomic DNA double-strand breaks (DSBs), while INK128 may mildly induce DDR in addition to oxidative stress. Consistently, the γ-H2AX levels in the drug combination group with NAC incubation were

moderately higher than those in the untreated group (Fig. 3I), indicating that INK128 can play an auxiliary role in enhancing CX5461-induced DNA-damaging stress. A former study reported that EVER can improve the anticancer effects of CX5461 on MYC-driven lymphoma by inducing the expression of proapoptotic protein BMF independent of the p53 pathway [32]. Collectively, INK128 may enhance the antitumor efficacy of CX5461 in a cell-type dependent manner.

3.3. INK128 suppressed NHEJ-DNA repair pathway to reinforce the effects of CX5461

Genomic stability is mostly maintained by the sophisticated DNA- damage repair system. When the cells are stimulated by internal and external stress to cause DDR, the homologous recombination (HR) and nonhomologous end joining (NHEJ) DNA repair pathways are activated to protect cells from apoptosis and aging. A recent study reported that the mTOR-S6K pathway regulated the DDR through E3 ubiquitin ligase RNF168 [12]. In addition, rDNA CNV is potentially attributable to NHEJ-DNA repair [13,46]. To further elucidate the synergistic mechanism of INK128 and CX5461, we detected protein expression of the DNA repair pathway. The γ-H2AX levels were gradually increased after 24 h of INK128 treatment in a dose-dependent manner (Fig. 4A and B). Here, we found that INK128 treatment did not have any effect on the expression of the NHEJ protein Ku80. Interestingly, the expression levels of Ku70 protein were markedly decreased by INK128 treatment in a dose-dependent manner (Fig. 4A and B). These data indicated that INK128 inhibited the Ku70-mediated NHEJ-DNA repair pathway, making the tumors more vulnerable to CX5461-induced DNA damage stress.

The DDR process has a series of events, including DNA-damage induction, cell cycle arrest, DNA replication and regulation, and DNA- damage repair, which ensure genome stability and cell survival [47]. To ensure the correct replication of genetic substances, strict cell cycle checkpoints are required for genome accuracy during cell division [48]. G2/M is the last checkpoint to protect cells from DNA damage. DNA-damaging stress activates the ATM−CHK2-CDC25 or
ATR− CHK1-CDC25 pathway to inhibit the activity of CDC2/Cyclin-B, and then prevent cells to enter into M phase [49]. As shown in Fig. S3E and F, the cell cycle progress of OSCC cells was obviously retarded at the G2/M stage, and the cell population was significantly reduced at the G1 stage by INK128 or CX5461 treatment, while the cell cycle retardation was remarkably more evident with the combined treatment, indicating that the coadministration produced a synergistic effect to suppress the cell cycle process. Phosphorylation of Tyr15 on the CDC2 protein inactivated CDC2 function to suppress cell mitosis and induce G2/M arrest [50]. To assess the effect of INK128 on this cell cycle-regulatory protein CDC2, Cal33 and HSC3 cells were treated with different concentration of INK128 for 24 h. The results showed that
INK128 treatment elevated the expression levels of phosphorylated-CDC2 protein in OSCC cells dose-dependently (Fig. 4C and D). Moreover, the combined treatment of INK128 and CX5461 synergistically induced the phosphorylation levels of Tyr15 on the CDC2 protein, but not the protein expression of Ku70 and Ku80 (Fig. 4E). These data are consistent with the cell cycle analysis.

Subsequently, we analyzed whether mTORC1/2 signaling indeed played an important role in the repair of CX5461-induced DNA DSB. The tumor cells were treated with CX5461 for 4 or 24 h in the presence or absence of INK128 to observe the effect of INK128 on DNA-damage repair. As expected, DDR was strongest after INK128 + CX5461 (24 h) treatment, and no significant differences were observed between the CX5461 (4 h) and CX5461 (0 h) -treated groups. However, DNA damage signaling after INK128 + CX5461 (4 h) treatment was significantly greater than that after long-term treatment with CX5461 (24 h) alone (Fig. 4F and G). These results clearly supported that DNA damage was repaired during the subsequent 20 h in fresh culture medium after a 4 -h pulse treatment with CX4561, but the DNA repair process was inhibited by INK128 in the combined treatment. Taken together, INK128 reinforced the antitumor activity of CX5461 through impeding the NHEJ- DNA repair pathway and cell cycle-regulatory protein CDC2.

3.4. In vivo therapeutic effects of CX5461 and INK128 in a mouse cancer model

We validated the therapeutic effects of CX5461 and INK128 *in vivo* in a tumor-xenograft mouse model. OSCC tumor xenografts were generated by subcutaneously injecting Cal33 cells into nude mice. Six days later, these tumor-bearing mice were randomly divided into four groups (n = 10) and were injected daily with the vehicle control, INK128, CX5461 or the combination of INK128 + CX5461 for 27 days. As shown in Fig. 5A–C, INK128 alone only moderately inhibited the growth of OSCC tumors (average tumor weight: 2.17 ± 0.16 g/mouse, p□0.001) compared with the vehicle control group (3.43 ± 0.21 g/mouse), while CX5461 had a stronger tumor-inhibition effect (average tumor weight: 1.52 ± 0.17 g/mouse, p□0.001) than INK128 for the *in vivo* growth of the tumors. As expected, the combined treatment synergized to robustly suppress the tumor growth (average tumor weight: 0.34 ± 0.06 g/mice, p□0.001). Consistently, the coadministration of INK128 and CX5461 reduced the tumor size compared with single- compound treatment (p□0.001, Fig. 5B). By Ki67-positive staining analysis, cell proliferation of the tumors was mostly inhibited by the combined treatment (average cell number with Ki67-positive staining: 85 ± 25, p□0.001) compared with the single-compound treatment and the vehicle control group (INK128-treated group: 208 ± 34, CX5461- treated group: 182 ± 57, the vehicle control group: 325 ± 42. Fig. 5D and E). In addition, CX5461 induced substantially more apoptosis of the tumors (apoptosis rate: 53.85 ± 5.34 %) than INK128 (apoptosis rate: 24.48 ± 6.22 %) and the vehicle control (apoptosis rate: 4.22 ± 2.12 %), and the coadministration displayed synergistic activity to robustly induce cell apoptosis *in vivo* (apoptosis rate: 72.78 ± 3.96 %), which was in good agreement with

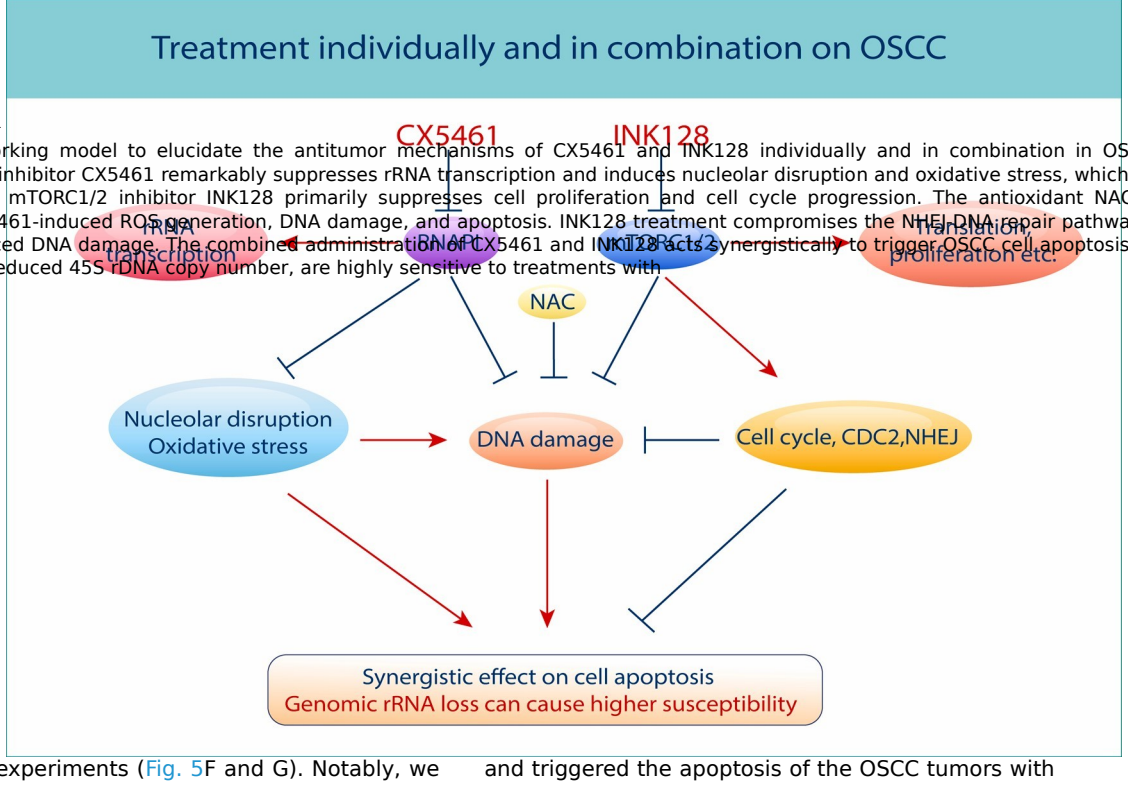

Fig. 6. A working model to elucidate the antitumor mechanisms of CX5461 and INK128 individually and in combination in OSCC. The RNA polymerase I inhibitor CX5461 remarkably suppresses rRNA transcription and induces nucleolar disruption and oxidative stress, which leads to DNA damage. The mTORC1/2 inhibitor INK128 primarily suppresses cell proliferation and cell cycle progression. The antioxidant NAC significantly prevents CX5461-induced ROS generation, DNA damage, and apoptosis. INK128 treatment compromises the NHEJ DNA repair pathway to reinforce CX5461-induced DNA damage. The combined administration of CX5461 and INK128 acts synergistically to trigger OSCC cell apoptosis. OSCC tumor cells, with a reduced 45S rDNA copy number, are highly sensitive to treatments with

the *in vitro* experiments (Fig. 5F and G). Notably, we did not observe any weight changes between the treatment groups (Fig. S5A).

Furthermore, we assessed the effects of the indicated treatments on the survival and cancer metastasis of the tumor-bearing mice. Excitingly, the combined treatment dramatically prolonged the lifespan of the tumor-bearing mice compared with the single-compound treatments (average survival time: 61 days in the INK128-treated group, 75 days in the CX5461-treated group) and the vehicle control group (average survival time: 48 days). Mice began to die on the 88th day, and six mice were dead at the 100th day in the group co-administration group (Fig. S5B). In addition, the combined treatment appeared to reduce the incidence of the enlarged inguinal lymph nodes *in vivo* in the mouse model (Fig. S5C and D). Additionally, we also observed the histology and morphology of kidney and liver tissues to evaluate adverse effects of these treatments (Fig. S5E). Neither the individual compounds nor the co-administration showed any toxicity to the kidney and liver of the tumor-bearing mice. Collectively, the findings strongly supported that the co-inhibition of RNAPI and mTORC1/2 is a novel efficient therapeutic strategy to improve the prognosis of OSCC.

4. Discussion

In this report, we found that 45S rDNA copy number was frequently reduced in primary OSCC tumors and was associated with the overexpression of mTOR activity. Both 45S and 28S rDNA regions have a higher variation of sequences, and at least 65 genes have the copy number covariations coupled with the partial loss of 45S rDNA repeats in the primary tumors. A combination of CX5461 and INK128 synergistically suppressed cell proliferation and colony formation, and induced cell apoptosis, ROS generation, nucleolar disorganization, and DNA-damaging *in vitro*. Furthermore, the combination of CX5461 and INK128 also exhibited synergistic therapeutic effects *in vivo* in the tumor-xenograft mouse model. In the animal experiments, we found that the cotreatment robustly prevented the growth and triggered the apoptosis of the OSCC tumors with few adverse effects. Intriguingly, the combined treatment dramatically extended the survival time of the tumor-bearing animals.

A few studies have reported that rDNA copies in yeast, nematodes, mice and humans are reduced along with cellular aging [51]. Because advanced tumors often exhibit malignant growth and proliferation,
CX5461 and coadministration of CX5461 and INK128.

cancer migration and lymph node metastasis, the late-stage primary OSCCs may have a higher probability of exhibiting increased cell division and cell senescence. Both factors could contribute to the reduction in rDNA copy number. Therefore, a partial loss of 45S rDNA copies might be useful to predict tumor progression.

Multiple mechanisms are involved in the resistance to mTOR inhibitors, such as the c-Myc, β-catenin, JAK/STAT, and MAPK pathways [52], and some mTOR inhibitors only mildly inhibit the downstream effector 4EBP1 [53]. Our results also indicated that INK128 significantly inhibited OSCC cell proliferation but did not induce cell apoptosis. In the whole-genome DNA-seq analysis, at least 65 genes have the copy number covariations coupled with the partial loss of 45S rDNA copies, and the rDNA regions exhibited a significantly higher variation in the primary OSCC tumors. These data indicated that the OSCC tumors, with rDNA copy loss, could have more heterogeneity to develop drug resistance to a single compound. Our study clearly illustrated that multiple colonies of OSCC cells produced obvious resistance to INK128 treatment by the single-cell colony-formation assay. Given these findings, mTOR inhibitors alone may be insufficient to treat OSCC tumors. ATRX (alpha thalassemia/mental retardation X-linked) mutations have been reported to contribute to the loss of rDNA copies and rDNA instability, leading to high sensitivity to CX5461 in ALT (alternative lengthening of telomeres)-positive cancers [39]. In agreement, our study also supported that OSCC tumors have substantially higher sensitivity to CX5461 associated

with a reduced copy number of 45S rDNA. Because rDNA copy loss may be associated with hyperactive PI3K-mTOR pathways, the coinhibition of mTORC1/2 and RNAPI is a plausible approach to treat OSCC tumors. Here, the data clearly demonstrated that mTORC1/2 inhibition has the capacity to enhance CX5461-induced ROS generation, DNA damage and nucleolar stress. The combined inhibition of rDNA transcription and Akt-mTOR signaling not only repressed ribosome biogenesis and protein translation, but also boosted the anticancer activity of the single agent.

Chemotherapeutic resistance is an obstacle for cancer treatment. All of the complicated compensation by oncogenic pathways, tumor heterogeneity and upregulated DNA repair contribute to chemotherapy failure [54]. A few mTOR inhibitors are reported to increase the sensitivity of tumors to radiation and chemotherapy [55]. Akt can phosphorylate PKCs to facilitate the DNA DSB repair pathway [56]. By immediate complex formation with DNA-dependent protein kinase catalytic subunit (DNA-PKcs), Akt can stimulate the accumulation of DNA-PKcs at the sites of DNA DSB and promote DNA-PKcs activity for efficient NHEJ-DNA DSB repair [56]. In the study, the data illustrated that the combination of CX5461 and INK128 synergistically retarded the cell cycle at the G2/M phase. In addition, the inhibition of Akt-mTOR signaling gradually triggered DNA DSBs, remarkably suppressed the NHEJ-DNA repair pathway, and caused inactivation of the cell cycle checkpoint protein CDC2 [57]. Thus, the study provided a rational interpretation regarding the underlying mechanism of
INK128-reinforced antitumor activity of CX5461.

TP53 mutations have recently been reported to correlate with 45S rDNA copy loss in several cancer types [58]. TP53 serves as a guardian of the genome to prevent the replication of damaged DNA [59]. Selective pressure on DNA replication in cancer cells tends to prefer fewer rDNA copies, allowing the genome to replicate faster and easier [60]. A few studies have revealed that chromosomal rDNA can convert into extrachromosomal rDNA circles via dissociation from the genome, and the RNAPI activator UAF may monitor and regulate rDNA CNV in the budding yeast model [61,62]. These reports indicate that a partial loss of genomic rDNA copies may be attributed to the accumulation and production of extrachromosomal rDNA circles in primary tumors. As the most abundant noncoding genes of the human genome, chromosomal rDNA may serve as a genome buffering system with a protective role against DNA-damaging stress and genome instability [63]. Thus, the reduction of rDNA copies could downsize the genomic abundance of the tumors, leading to a fast DNA replication and increased susceptibility to genomic instability.

Furthermore, the study demonstrated that the combination of CX5461 and INK128 exhibited synergistic therapeutic effects *in vivo* in a mouse cancer model. In animal experiments, the coadministration robustly prevented the growth and proliferation of OSCC tumors, and triggered striking levels of apoptosis with few adverse effects. Intriguingly, the combined treatment dramatically extended the survival time of the tumor-bearing animals and reduce the incidences of the enlarged inguinal lymph nodes. Thus, our data clearly revealed that the cotargeting of RNAPI transcription and Akt/mTOR signaling was highly effective at treating the malignant tumors. To our knowledge, we are the first group to demonstrate that targeting ribosome biogenesis and protein translation simultaneously can be exploited therapeutically in both *in vivo* and *in vitro* models of OSCC.

In summary, we provided a working model to elucidate the mechanisms of CX5461 and INK128 to combat OSCC tumors, individually and in combination (Fig. 6). The combination therapy was efficacious across different OSCC cells and primary tumors featuring dysregulation of mTOR signaling as well as rDNA copy loss. INK128 treatment exhibits a highly cooperative action with CX5461 through the inhibition of cell cycle progression and NHEJ-DNA repair pathway, and the induction of DNA damaging and nucleolar stress. Although OSCC tumors are complicatedly mutated at multiple oncogenes and are heterogeneous, the partial loss of 45S rDNA repeats may serve as a potent index to predict the efficiency and response of the cotargeting therapy. The findings are significant as they demonstrate that rRNA transcription and mTORC1/2 signaling are profoundly cooperative in oral cancers to drive cancer addiction to ribosome biogenesis and protein translation. The study supports the potential treatment of CX5461 and INK128 coadministration to treat the malignant tumors, especially in those with a reduction in 45S rDNA copy number. The work can provide a novel therapeutic option to improve the prognosis of oral cancers.

Funding

The study was supported by the grants No. 81771056 (BX), No. 81972533 (BX), No. 81672679 (GL), No. 81972532 (ZW), No. 81772896 (ZW) from National Natural Science Foundation of China (http://www.nsfc.gov.cn/english/site_1/index.html), and Start-up funding from the hundred talent program of hospital of stomatology at the Sun Yat-sen University. The work was also supported by Open Funding of Guangdong Provincial Key Laboratory of Stomatology (KF2018120104), and Open Funding of State Key Laboratory of Oral Diseases at Sichuan University (SKLOD2020OF03 to BX), and Guangdong Financial fund for High-Caliber Hospital Construction (174-2018- XMZC-0001-03-0125/D-13), and the Fundamental Research Funds for the Central Universities, Sun Yat-sen University (20ykzd09 to BX). The sponsors or funders did not play any role in the study design, data collection and analysis, decision to publish, or preparation of the manuscript.

Data availability

The original datasets are available from the corresponding author upon request.

Declaration of Competing Interest

The authors reported no declarations of interest.

Acknowledgements

We are thankful to the Molecular Biology, Flow Cytometry, Tissue Culture, and Microscopy core facilities at the Guangdong Provincial Key Laboratory of Stomatology for enabling many of our experiments. We thank members of the Gerton laboratory at Stowers Institute for helpful discussions. We are grateful to Zhi Wang, Bin Cheng, Juan Xia, Guiqing Liao, Yujie Liang and Yun Wang for tissue samples and essential reagents. We sincerely thank Dr. Jennifer L. Gerton for important assistance. We thank Hua Li for help with bioinformatics analysis and Edmund Howe with PCR assistance. We thank Yihan Xing for the preparation of buffer and reagents.

Appendix A. Supplementary data

Supplementary material related to this article can be found, in the online version, at doi:https://doi.org/10.1016/j.biopha.2020.110906.

References

[1] S. Marcazzan, E.M. Varoni, E. Blanco, G. Lodi, M. Ferrari, Nanomedicine, an emerging therapeutic strategy for oral cancer therapy, Oral Oncol. 76 (2018) 1–7, https://doi.org/10.1016/j.oraloncology.2017.11.014.

[2] N. Vigneswaran, M.D. Williams, Epidemiologic trends in head and neck cancer and aids in diagnosis, Oral Maxillofac. Surg. Clin. N. Am. 26 (2014) 123–141, https://doi.org/10.1016/j.coms.2014.01.001.

[3] B. Mansoori, A. Mohammadi, S. Davudian, S. Shirjang, B. Baradaran, The different mechanisms of cancer drug resistance: a brief review, Adv. Pharm. Bull. 7 (2017) 339–348, https://doi.org/10.15171/apb.2017.041.

[4] C. Wang, X.Q. Liu, J.S. Hou, J.N. Wang, H.Z. Huang, Molecular mechanisms of chemoresistance in oral cancer, Chin. J. Dent. Res. 19 (2016) 25–33, https://doi.org/10.3290/j.cjdr.a35694.

[5] M. Wang, B. Lemos, Ribosomal DNA copy number amplification and loss in human cancers is linked to tumor genetic context, nucleolus activity, and proliferation, PLoS Genet. 13 (2017), e1006994, https://doi.org/10.1371/journal.pgen.1006994.

[6] M. Laplante, D.M. Sabatini, mTOR signaling in growth control and disease, Cell 149 (2012) 274–293, https://doi.org/10.1016/j.cell.2012.03.017.

[7] J.L. Sebaugh, Guidelines for accurate EC50/IC50 estimation, Pharm. Stat. 10 (2011) 128–134, https://doi.org/10.1002/pst.426.

[8] D. Chen, S. Huang, Nucleolar components involved in ribosome biogenesis cycle between the nucleolus and nucleoplasm in interphase cells, J. Cell Biol. 153 (2001) 169–176, https://doi.org/10.1083/jcb.153.1.169.

[9] Y. Zhang, D. Qian, Z. Li, Y. Huang, Q. Wu, G. Ru, M. Chen, B. Wang, Oxidative stress-induced DNA damage of mouse zygotes triggers G2/M checkpoint and phosphorylates Cdc25 and Cdc2, Cell Stress Chaperones 21 (2016) 687–696, https://doi.org/10.1007/s12192-016-0693-5.

[10] C.F. Malone, C. Emerson, R. Ingraham, W. Barbosa, S. Guerra, H. Yoon, L.L. Liu, F. Michor, M. Haigis, K.F. Macleod, O. Maertens, K. Cichowski, mTOR and HDAC inhibitors converge on the TXNIP/thioredoxin pathway to cause catastrophic oxidative stress and regression of RAS-driven tumors, Cancer Discov. 7 (2017) 1450–1463, https://doi.org/10.1158/2159-8290.CD-17-0177.

[11] M. Li, L. You, J. Xue, Y. Lu, Ionizing radiation-induced cellular senescence in normal, non-transformed cells and the involved DNA damage response: a mini review, Front. Pharmacol. 9 (2018) 522, https://doi.org/10.3389/fphar.2018.00522.

[12] X. Xie, H. Hu, X. Tong, L. Li, X. Liu, M. Chen, H. Yuan, X. Xie, Q. Li, Y. Zhang, H. Ouyang, M. Wei, J. Huang, P. Liu, W. Gan, Y. Liu, A. Xie, X. Kuai, G.W. Chirn, H. Zhou, R. Zeng, R. Hu, J. Qin, F.L. Meng, W. Wei, H. Ji, D. Gao, The mTOR-S6K pathway links growth signalling to DNA damage response by targeting RNF168, Nat. Cell Biol. 20 (2018) 320–331, https://doi.org/10.1038/s41556-017-0033-8.

[13] T. Miyoshi, J. Kanoh, F. Ishikawa, Fission yeast Ku protein is required for recovery from DNA replication stress, Genes Cells 14 (2009) 1091–1103, https://doi.org/ 10.1111/j.1365-2443.2009.01337.x.

[14] X. Li, C. Wu, N. Chen, H. Gu, A. Yen, L. Cao, E. Wang, L. Wang, PI3K/Akt/mTOR signaling pathway and targeted therapy for glioblastoma, Oncotarget 7 (2016) 33440–33450, https://doi.org/10.18632/oncotarget.7961.

[15] M. Pierobon, C. Ramos, S. Wong, K.A. Hodge, J. Aldrich, S. Byron, S.P. Anthony, N. J. Robert, D.W. Northfelt, M. Jahanzeb, L. Vocila, J. Wulfkuhle, G. Gambara, R. I. Gallagher, B. Dunetz, N. Hoke, T. Dong, D.W. Craig, M. Cristofanilli, B. Leyland- Jones, L.A. Liotta, J.A. O'Shaughnessy, J.D. Carpten, E.F. Petricoin, Enrichment of PIK3-AKT-MTOR pathway activation in hepatic metastases from breast cancer, Clin. Cancer Res. 23 (2017) 4919–4928, https://doi.org/10.1158/1078-0432.CCR- 16-2656.

[16] M.L. Hedberg, V. Lui, H. Li, B. Vangara, K. Pendleton, Y. Zeng, B. Gilbert, M. Freilino, S. Sauerwein, N. Peyser, B. Diergaarde, P. Hammerman, L. Garraway, G. Mills, J. Grandis, Abstract 2011: the PI3K pathway is the most frequently mutated mitogenic pathway in HNSCC, Cancer Res. 73 (2013) 2011, https://doi. org/10.1158/1538-7445.am2013-2011.

[17] D. Horn, J. Hess, K. Freier, J. Hoffmann, C. Freudlsperger, Targeting EGFR-PI3K- AKT-mTOR signaling enhances radiosensitivity in head and neck squamous cell carcinoma, Expert Opin. Ther. Targets 19 (2015) 795–805, https://doi.org/ 10.1517/14728222.2015.1012157.

[18] J.E. Bauman, H. Arias-Pulido, S.J. Lee, M.H. Fekrazad, H. Ozawa, E. Fertig, J. Howard, J. Bishop, H. Wang, G.T. Olson, M.J. Spafford, D.V. Jones, C.H. Chung, A phase II study of temsirolimus and erlotinib in patients with recurrent and/or metastatic, platinum-refractory head and neck squamous cell carcinoma, Oral Oncol. 49 (2013) 461–467, https://doi.org/10.1016/j.oraloncology.2012.12.016.

[19] Z.J. Sun, L. Zhang, B. Hall, Y. Bian, J.S. Gutkind, A.B. Kulkarni, Chemopreventive and chemotherapeutic actions of mTOR inhibitor in genetically defined head and neck squamous cell carcinoma mouse model, Clin. Cancer Res. 18 (2012) 5304–5313, https://doi.org/10.1158/1078-0432.ccr-12-1371.

[20] A. Herzog, Y. Bian, R. Vander Broek, B. Hall, J. Coupar, H. Cheng, A.L. Sowers, J. D. Cook, J.B. Mitchell, Z. Chen, A.B. Kulkarni, C. Van Waes, PI3K/mTOR inhibitor PF-04691502 antitumor activity is enhanced with induction of wild-type TP53 in human xenograft and murine knockout models of head and neck cancer, Clin. Cancer Res. 19 (2013) 3808–3819, https://doi.org/10.1158/1078-0432.ccr-12- 2716.

[21] V. Patel, C.A. Marsh, R.T. Dorsam, C.M. Mikelis, A. Masedunskas, P. Amornphimoltham, C.A. Nathan, B. Singh, R. Weigert, A.A. Molinolo, J. S. Gutkind, Decreased lymphangiogenesis and lymph node metastasis by mTOR inhibition in head and neck cancer, Cancer Res. 71 (2011) 7103–7112, https://doi.org/10.1158/0008-5472.can-10-3192.

[22] A.A. Molinolo, C. Marsh, M. El Dinali, N. Gangane, K. Jennison, S. Hewitt, V. Patel, T.Y. Seiwert, J.S. Gutkind, mTOR as a molecular target in HPV-associated oral and cervical squamous carcinomas, Clin. Cancer Res. 18 (2012) 2558–2568, https:// doi.org/10.1158/1078-0432.ccr-11-2824.

[23] X. Wu, H. Yeerna, Y. Goto, T. Ando, V.H. Wu, X. Zhang, Z. Wang, P. Amornphimoltham, A.N. Murphy, P. Tamayo, Q. Chen, S.M. Lippman, J. S. Gutkind, Metformin inhibits progression of head and neck squamous cell carcinoma by acting directly on carcinoma-initiating cells, Cancer Res. 79 (2019) 4360–4370, https://doi.org/10.1158/0008-5472.CAN-18-3525.

[24] X. Liang, M. Deng, C. Zhang, F. Ping, H. Wang, Y. Wang, Z. Fan, X. Ren, X. Tao, T. Wu, J. Xu, B. Cheng, J. Xia, Combined class I histone deacetylase and mTORC1/ C2 inhibition suppresses the initiation and recurrence of oral squamous cell carcinomas by repressing SOX2, Cancer Lett. 454 (2019) 108–119, https://doi.org/10.1016/j.canlet.2019.04.010.

[25] B. Albert, I. Leger-Silvestre, C. Normand, M.K. Ostermaier, J. Perez-Fernandez, K. I. Panov, J.C. Zomerdijk, P. Schultz, O. Gadal, RNA polymerase I-specific subunits promote polymerase clustering to enhance the rRNA gene transcription cycle, J. Cell Biol. 192 (2011) 277–293, https://doi.org/10.1083/jcb.201006040.

[26] H. Suzuki, S. Sakurai, Y. Matsuda, Rat 5S rDNA spacer sequences and chromosomal assignment of the genes to the extreme terminal region of chromosome 19, Cytogenet. Cell Genet. 72 (1996) 1–4, https://doi.org/10.1159/000134149.

[27] C. Fernandez-Tornero, B. Bottcher, M. Riva, C. Carles, U. Steuerwald, R.
W. Ruigrok, A. Sentenac, C.W. Muller, G. Schoehn, Insights into transcription initiation and termination from the electron microscopy structure of yeast RNA polymerase III, Mol. Cell 25 (2007) 813–823, https://doi.org/10.1016/j.molcel.2007.02.016.
[28] J. Pelletier, G. Thomas, S. Volarevic, Ribosome biogenesis in cancer: new players and therapeutic avenues, Nat. Rev. Cancer 18 (2018) 51–63, https://doi.org/10.1038/nrc.2017.104.
[29] M. Haddach, M.K. Schwaebe, J. Michaux, J. Nagasawa, S.E. O'Brien, J.P. Whitten,
F. Pierre, P. Kerdoncuff, L. Darjania, R. Stansfield, D. Drygin, K. Anderes,
C. Proffitt, J. Bliesath, A. Siddiqui-Jain, M. Omori, N. Huser, W.G. Rice, D.
M. Ryckman, Discovery of CX-5461, the first direct and selective inhibitor of RNA polymerase I, for cancer therapeutics, ACS Med. Chem. Lett. 3 (2012) 602–606, https://doi.org/10.1021/ml300110s.
[30] H.C. Lee, H. Wang, V. Baladandayuthapani, H. Lin, J. He, R.J. Jones, I. Kuiatse, D. Gu, Z. Wang, W. Ma, J. Lim, S. O'Brien, J. Keats, J. Yang, R.E. Davis, R.
Z. Orlowski, RNA polymerase I inhibition with CX-5461 as a novel therapeutic strategy to target MYC in multiple myeloma, Br. J. Haematol. 177 (2017) 80–94, https://doi.org/10.1111/bjh.14525.
[31] A.W.Y. Leung, M. Anantha, K.E. Prosser, M. Wehbe, C.J. Walsby, M.B. Bally,
Abstract 1319: a novel formulation of CX-5461, a small-molecule inhibitor of rRNA synthesis, and its use for treatment of acute myeloid leukemia models, Cancer Res. 76 (2016) 1319, https://doi.org/10.1158/1538-7445.am2016-1319.
[32] J.R. Devlin, K.M. Hannan, N. Hein, C. Cullinane, E. Kusnadi, P.Y. Ng, A.J. George, J. Shortt, M.J. Bywater, G. Poortinga, E. Sanij, J. Kang, D. Drygin, S. O'Brien, R. W. Johnstone, G.A. McArthur, R.D. Hannan, R.B. Pearson, Combination therapy targeting ribosome biogenesis and mRNA translation synergistically extends survival in MYC-driven lymphoma, Cancer Discov. 6 (2016) 59–70, https://doi.org/10.1158/2159-8290.CD-14-0673.
[33] H. Xu, M. Di Antonio, S. McKinney, V. Mathew, B. Ho, N.J. O'Neil, N.D. Santos, J. Silvester, V. Wei, J. Garcia, F. Kabeer, D. Lai, P. Soriano, J. Banath, D.S. Chiu,
D. Yap, D.D. Le, F.B. Ye, A. Zhang, K. Thu, J. Soong, S.C. Lin, A.H. Tsai, T. Osako, T. Algara, D.N. Saunders, J. Wong, J. Xian, M.B. Bally, J.D. Brenton, G.W. Brown,
S.P. Shah, D. Cescon, T.W. Mak, C. Caldas, P.C. Stirling, P. Hieter,
S. Balasubramanian, S. Aparicio, CX-5461 is a DNA G-quadruplex stabilizer with selective lethality in BRCA1/2 deficient tumours, Nat. Commun. 8 (2017) 14432, https://doi.org/10.1038/ncomms14432.
[34] P.M. Bruno, M. Lu, K.A. Dennis, H. Inam, C.J. Moore, J. Sheehe, S.J. Elledge, M. T. Hemann, J.R. Pritchard, The primary mechanism of cytotoxicity of the chemotherapeutic agent CX-5461 is topoisomerase II poisoning, Proc. Natl. Acad. Sci. U. S. A. 117 (2020) 4053–4060, https://doi.org/10.1073/pnas.1921649117.
[35] S. Li, S. Zhang, J. Chen, c-Myc induced upregulation of long non-coding RNA SNHG16 enhances progression and carcinogenesis in oral squamous cell carcinoma, Cancer Gene Ther. 26 (2019) 400–410, https://doi.org/10.1038/s41417-018-0072-8.
[36] W. Zhao, Y. Cui, L. Liu, X. Qi, J. Liu, S. Ma, X. Hu, Z. Zhang, Y. Wang, H. Li, Z. Wang, Z. Liu, J. Wu, Splicing factor derived circular RNA circUHRF1 accelerates oral squamous cell carcinoma tumorigenesis via feedback loop, Cell Death Differ. 27 (2020) 919–933, https://doi.org/10.1038/s41418-019-0423-5.
[37] B. Xu, H. Li, J.M. Perry, V.P. Singh, J. Unruh, Z. Yu, M. Zakari, W. McDowell, L. Li, J.L. Gerton, Ribosomal DNA copy number loss and sequence variation in cancer, PLoS Genet. 13 (2017), e1006771, https://doi.org/10.1371/journal.pgen.1006771.
[38] A.V. Cerqueira, B. Lemos, Ribosomal DNA and the nucleolus as keystones of nuclear architecture, organization, and function, Trends Genet. 35 (2019) 710–723, https://doi.org/10.1016/j.tig.2019.07.011.
[39] M. Udugama, E. Sanij, H.P.J. Voon, J. Son, L. Hii, J.D. Henson, F.L. Chan, F.T.
M. Chang, Y. Liu, R.B. Pearson, P. Kalitsis, J.R. Mann, P. Collas, R.D. Hannan, L. H. Wong, Ribosomal DNA copy loss and repeat instability in ATRX-mutated cancers, Proc. Natl. Acad. Sci. U. S. A. 115 (2018) 4737–4742, https://doi.org/10.1073/pnas.1720391115.
[40] M. Mandrioli, M.S. Colomba, R. Vitturi, Chromosomal analysis of repeated DNAs in the rainbow wrasse *Coris julis* (Pisces, Labridae), Genetica 108 (2000) 191–195, https://doi.org/10.1023/a:1004199902680.
[41] T. Bose, K.K. Lee, S. Lu, B. Xu, B. Harris, B. Slaughter, J. Unruh, A. Garrett, W. McDowell, A. Box, H. Li, A. Peak, S. Ramachandran, C. Seidel, J.L. Gerton, Cohesin proteins promote ribosomal RNA production and protein translation in yeast and human cells, PLoS Genet. 8 (2012), e1002749, https://doi.org/10.1371/ journal.pgen.1002749.
[42] V. Iadevaia, Z. Zhang, E. Jan, C.G. Proud, mTOR signaling regulates the processing of pre-rRNA in human cells, Nucleic Acids Res. 40 (2012) 2527–2539, https://doi.org/10.1093/nar/gkr1040.
[43] C. Mayer, I. Grummt, Ribosome biogenesis and cell growth: mTOR coordinates transcription by all three classes of nuclear RNA polymerases, Oncogene 25 (2006) 6384–6391, https://doi.org/10.1038/sj.onc.1209883.
[44] J.G. Gibbons, A.T. Branco, S. Yu, B. Lemos, Ribosomal DNA copy number is coupled with gene expression variation and mitochondrial abundance in humans, Nat. Commun. 5 (2014) 4850, https://doi.org/10.1038/ncomms5850.
[45] S. Ide, T. Miyazaki, H. Maki, T. Kobayashi, Abundance of ribosomal RNA gene copies maintains genome integrity, Science 327 (2010) 693–696, https://doi.org/10.1126/science.1179044.
[46] Y. Yu, N. Pham, B. Xia, A. Papusha, G. Wang, Z. Yan, G. Peng, K. Chen, G. Ira, Dna2 nuclease deficiency results in large and complex DNA insertions at chromosomal breaks, Nature 564 (2018) 287–290, https://doi.org/10.1038/s41586-018-0769-8.
[47] W. Liu, J. Li, Y.S. Song, Y. Li, Y.H. Jia, H.D. Zhao, Cdk5 links with DNA damage response and cancer, Mol. Cancer 16 (2017) 60, https://doi.org/10.1186/s12943- 017-0611-1.
[48] R. Roy, D. Pal, S. Sur, S. Mandal, P. Saha, C.K. Panda, Pongapin and Karanjin, furanoflavanoids of *Pongamia pinnata*, induce G2/M arrest and apoptosis in cervical cancer cells by differential reactive oxygen species modulation, DNA damage, and nuclear factor kappa-light-chain-enhancer of activated B cell signaling, Phytother. Res. 33 (2019) 1084–1094, https://doi.org/10.1002/ptr.6302.
[49] J. Smith, L.M. Tho, N. Xu, D.A. Gillespie, The ATM-Chk2 and ATR-Chk1 pathways in DNA damage signaling and cancer, Adv. Cancer Res. 108 (2010) 73–112, https://doi.org/10.1016/B978-0-12-380888-2.00003-0.
[50] S. Wu, S. Zheng, S. Wang, W.K.A. Yung, D. Koul, Abstract 31: WEE1 kinase inhibition enhances PI3K inhibitor response in p53 deficient gliomas, Cancer Res.
75 (2015) 31, https://doi.org/10.1158/1538-7445.am2015-31.
[51] B. Li, K.A.G. Kremling, P. Wu, R. Bukowski, M.C. Romay, E. Xie, E.S. Buckler, M. Chen, Coregulation of ribosomal RNA with hundreds of genes contributes to phenotypic variation, Genome Res. 28 (2018) 1555–1565, https://doi.org/10.1101/gr.229716.117.
[52] E.A. El-Habr, G. Levidou, E.A. Trigka, J. Sakalidou, C. Piperi, I. Chatziandreou,
A. Spyropoulou, R. Soldatos, G. Tomara, K. Petraki, V. Samaras, A. Zisakis,
V. Varsos, G. Vrettakos, E. Boviatsis, E. Patsouris, A.A. Saetta, P. Korkolopoulou,
Complex interactions between the components of the PI3K/AKT/mTOR pathway, and with components of MAPK, JAK/STAT and Notch-1 pathways, indicate their involvement in meningioma development, Virchows Arch. 465 (2014) 473–485, https://doi.org/10.1007/s00428-014-1641-3.
[53] C. Baumann, A. Ullrich, R. Torka, GAS6-expressing and self-sustaining cancer cells in 3D spheroids activate the PDK-RSK-mTOR pathway for survival and drug resistance, Mol. Oncol. 11 (2017) 1430–1447, https://doi.org/10.1002/1878-0261.12109.
[54] D.C. Dartsch, F. Gieseler, Repair of idarubicin-induced DNA damage: a cause of resistance? DNA Repair (Amst) 6 (2007) 1618–1628, https://doi.org/10.1016/j. dnarep.2007.05.007.
[55] T.J. Hayman, A. Wahba, B.H. Rath, H. Bae, T. Kramp, U.T. Shankavaram, K. Camphausen, P.J. Tofilon, The ATP-competitive mTOR inhibitor INK128 enhances *in vitro* and *in vivo* radiosensitivity of pancreatic carcinoma cells, Clin. Cancer Res. 20 (2014) 110–119, https://doi.org/10.1158/1078-0432.CCR-13- 2136.
[56] M. Toulany, K.J. Lee, K.R. Fattah, Y.F. Lin, B. Fehrenbacher, M. Schaller, B.P. Chen, D.J. Chen, H.P. Rodemann, Akt promotes post-irradiation survival of human tumor cells through initiation, progression, and termination of DNA-PKcs-dependent DNA double-strand break repair, Mol. Cancer

Res. 10 (2012) 945–957, https://doi.org/ 10.1158/1541-7786.MCR-11-0592.
[57] L. Chang, P.H. Graham, J. Hao, J. Ni, J. Bucci, P.J. Cozzi, J.H. Kearsley, Y. Li, PI3K/ Akt/mTOR pathway inhibitors enhance radiosensitivity in radioresistant prostate cancer cells through inducing apoptosis, reducing autophagy, suppressing NHEJ and HR repair pathways, Cell Death Dis. 5 (2014), e1437, https://doi.org/ 10.1038/cddis.2014.415.
[58] H.D. Hosgood, W. Hu, N. Rothman, M. Klugman, S.J. Weinstein, J.R. Virtamo, D. Albanes, R. Cawthon, Q. Lan, Variation in ribosomal DNA copy number is associated with lung cancer risk in a prospective cohort study, Carcinogenesis 40 (2019) 975–978, https://doi.org/10.1093/carcin/bgz052.
[59] J. Zhou, C. Prives, Replication of damaged DNA *in vitro* is blocked by p53, Nucleic Acids Res. 31 (2003) 3881–3892, https://doi.org/10.1093/nar/gkg468.
[60] A. Dereli-Oz, G. Versini, T.D. Halazonetis, Studies of genomic copy number changes in human cancers reveal signatures of DNA replication stress, Mol. Oncol. 5 (2011) 308–314, https://doi.org/10.1016/j.molonc.2011.05.002.
[61] A. Mansisidor, T. Molinar, P. Srivastava, D.D. Dartis, A. Pino Delgado, H. G. Blitzblau, H. Klein, A. Hochwagen, Genomic copy-number loss is rescued by self- limiting production of DNA circles, Mol. Cell 72 (2018) 3, https://doi.org/ 10.1016/j.molcel.2018.08.036.
[62] T. Iida, T. Kobayashi, RNA polymerase I activators count and adjust ribosomal RNA gene copy number, Mol. Cell 73 (2019) 4, https://doi.org/10.1016/j. molcel.2018.11.029.
[63] T. Kobayashi, M. Sasaki, Ribosomal DNA stability is supported by many' buffer genes'-introduction to the yeast rDNA stability database, FEMS Yeast Res. 17 (2017), fox001, https://doi.org/10.1093/femsyr/fox001.